High-frequency thermoelectric response in correlated electronic systems

Wenhu Xu, Cédric Weber, and Gabriel Kotliar

Phys. Rev. B **84**, 035114 — Published 21 July 2011

DOI: 10.1103/PhysRevB.84.035114

High frequency thermoelectric response in correlated electronic systems

Wenhu Xu,[1] Cédric Weber,[2] and Gabriel Kotliar[1]

[1] *Department of Physics and Astronomy, Rutgers University 136 Frelinghuysen Rd., Piscataway, NJ 08854, USA*

[2] *Cavendish Laboratories, Cambridge University, JJ Thomson Avenue, Cambridge, UK*

We derive a general formalism for evaluating the high-frequency limit of the thermoelectric power of strongly correlated materials, which can be straightforwardly implemented in available first principles LDA+DMFT programs. We explore this formalism using model Hamiltonians and we investigate the validity of approximating the static thermoelectric power S_0, by its high-temperature limit, S^*. We point out that the behaviors of S^* and S_0 are qualitatively different for a correlated Fermi liquid near the Mott transition, when the temperature is in the coherent regime. When the temperature is well above the coherent regime, e.g., when the transport is dominated by incoherent excitations, S^* provides a good estimation of S_0.

PACS numbers: 71.10.-w, 71.15.-m, 72.15.Jf

I. INTRODUCTION

Thermoelectric energy harvesting, i.e. the transformation of waste heat into usable electricity, is of great current interest. The main obstacle is the low efficiency of materials for converting heat to electricity[1,2]. Over the past decade, there has been a renewed interest on thermoelectric materials, mainly driven by experimental results[3].

Computing the thermoelectric power (TEP) in correlated systems is a highly non-trivial task and several approximation schemes have been used to this intent. The well-known Mott-Heikes formula[4,5] gives an estimate of the high temperature limit of TEP[6] in the strongly correlated regime. A generalized Boltzmann approach including vertex corrections has been developed in Ref.[7] and applied to several materials. Thermoelectric transport at intermediate temperature was carefully investigated in the context of single-band and degenerate Hubbard Hamiltonians, by dynamical mean field theory (DMFT)[8–10]. Kelvin formula was also revisited for various correlated models in Ref.[11] very recently.

The high frequency (AC) limit provides another interesting insights to gain further understanding of the thermoelectric transport in correlated materials, and is the main interest of this work. The thermopower in the high frequency limit of a degenerate Hubbard model near half-filling was considered in Ref.[9], where the authors generalize the thermoelectric response to finite frequencies in the high temperature limit. The same limit was studied recently by Shastry and collaborators, who have developed a formalism for evaluating the AC limit of thermoelectric response using high temperature series expansion and exact diagonalization. The methodology was applied to a single band t-J model on a triangular lattice[12,13]. The authors pointed out that the AC limit of TEP (S^*) is simple enough that it can be obtained by theoretical calculations with significantly less effort, while still provides nontrivial informations of the thermoelectric properties, and give an estimation of the trend of S_0.

In this work, we investigate the high frequency limit of TEP, S^*, by deriving an exact formalism in the context of a general multi-band model with local interactions. We show that S^* is determined by the bare band structure and the single-particle spectral functions. The relation between the conventional TEP, i.e., obtained at zero frequency (S_0) and the AC limit S^* is discussed from general arguments on the single particle properties of correlated systems at low and high temperatures. The analytical derivation of S^* is compared with the frequency dependent thermopower of the one band Hubbard model, solved by dynamical mean field theory (DMFT) on the square and triangular lattices. The formalism derived in this work can be conveniently implemented into first-principles calculations of realistic materials, such as in the LDA+DMFT framework[14,15].

This paper is organized as follows. In Sec. II A, general formalism of dynamical thermoelectric transport coefficients is summarized to define the notation. In Sec. II B, exact formulae to evaluate S^* are derived for a general tight-binding model with local interactions. In Sec. III, we apply the formalism to one-band Hubbard model on square and triangular lattice. The low and high temperature limit behaviors of S^* are discussed and compared to those of S_0. Numerical results are presented in Sec. IV. Sec. V summarizes the paper.

II. DYNAMICAL THERMOELECTRIC TRANSPORT FUNCTIONS AND HIGH-FREQUENCY LIMIT OF THERMOPOWER

A. General formalism

Electrical current can be induced by gradient of electrical potential and temperature. The phenomenological equations for static(DC limit) external fields are[16]

$$J_1^x = L_{11}^{xx}\left(-\frac{1}{T}\nabla_x\tilde{\mu}\right) + L_{12}^{xx}\left(\nabla_x\frac{1}{T}\right), \tag{1}$$

$$J_2^x = L_{21}^{xx}\left(-\frac{1}{T}\nabla_x\tilde{\mu}\right) + L_{22}^{xx}\left(\nabla_x\frac{1}{T}\right). \tag{2}$$

We only consider the longitudinal case. J_1^x and J_2^x are $x-$ component of particle and heat current, respectively. $\nabla_x\tilde{\mu}$ and $\nabla_x\frac{1}{T}$ are generalized forces driving J_1^x and J_2^x. $\tilde{\mu}=\mu-eV$, in which μ is chemical potential and V is the electric potential. L_{ij}^{xx} are transport coefficients. We follow the definition in Ref.[16], which explicitly respects the Onsager relation, $L_{ij}^{xx}=L_{ji}^{xx}$. Transport properties can be defined in terms of L_{ij}^{xx}. For example, the electric conductivity σ, thermoelectric power S, and the thermal conductivity κ are

$$\sigma = \frac{e^2}{T}L_{11}^{xx}, \tag{3}$$

$$S = -\frac{1}{eT}\frac{L_{12}^{xx}}{L_{11}^{xx}}, \tag{4}$$

$$\kappa = \frac{1}{T^2}\left(L_{22}^{xx}-\frac{(L_{12}^{xx})^2}{L_{11}^{xx}}\right). \tag{5}$$

In following context, we use $k_B = e = \hbar = 1$. The practical value of S is recovered by multiplying the factor $k_B/e = 86.3\mu V/K$, which we use as the unit for thermopower.

In conventional thermoelectric problems, L_{xx}^{ij} is theoretically defined and experimentally measured at the DC limit. The extension to dynamical(frequency) case is absent in standard textbooks but has been studied in detail in Ref.[12]. Here we give the outlines of the formalism. Borrowed from Luttinger's derivation[17], an auxiliary "gravitational" field coupled to energy density is defined. An "equivalence" between the fictitious gravitational field and the temperature gradient is proved. Then the transport coefficients L_{ij}^{xx} can be written in terms of correlation functions between particle current and(or) energy current. In Ref.[12], this formalism is generalized to temporally and spatially periodic external fields, thus the transport coefficients become momentum- and frequency-dependent functions, $L_{ij}^{xx}(\mathbf{q},\omega)$.

Some interesting remarks can be made on $L_{ij}^{xx}(\mathbf{q},\omega)$. On the one hand, in the DC limit($\omega\to 0$), there are two different ways of taking the thermodynamic limit($\mathbf{q}\to 0$)[12,17] because the two limits, $\omega\to 0$ and $\mathbf{q}\to 0$ do not commute. If we define $v=\frac{\omega}{|\mathbf{q}|}$ as the "phase velocity" of the external perturbation field, the so-called "fast limit" is defined as taking $\mathbf{q}\to 0$ before $\omega\to 0$, thus leading to $v\to\infty$. In the fast limit, the transport thermopower, or, the conventional DC limit of thermopower is obtained. The "slow limit" is defined as $\omega\to 0$ is taken before $\mathbf{q}\to 0$, thus $v\to 0$. Therefore, the perturbation is adiabatic and the charge and energy can redistribute to reach an equilibrium state. The slow limit then gives the Kelvin formula of thermopower discussed in Ref.[11].

On the other hand, in the AC limit($\omega\to\infty$), the two limits, $\omega\to\infty$ and $\mathbf{q}\to 0$, commute, because the phase velocity v will be infinity in either scenario. This can also be shown from the general formalism of $L_{ij}^{xx}(\mathbf{q},\omega)$ for finite $\mathbf{q}$ and ω in Ref.[12].

The dynamical transport coefficients with $\mathbf{q}\to 0$ are given by,

$$L_{ij}^{xx}(\omega) = T\int_0^\infty dt e^{i(\omega+i0^+)t}\int_0^\beta d\tau\langle J_j^x(-t-i\tau)J_i^x\rangle. \tag{6}$$

For a given Hamiltonian H, the current operators are defined by following the conservation laws[16],

$$J_i^x = \frac{\partial O_i^x}{\partial t} = i[H,O_i^x]. \tag{7}$$

O_i^x is the x-component of particle and heat polarization operator. Specifically,

$$O_1^x = \sum_i R_i^x n_i, \tag{8}$$

$$O_2^x = \sum_i R_i^x\left(h_i-\mu n_i\right), \tag{9}$$

where n_i and h_i are local particle and energy density operators. The explicit forms of n_i and h_i are determined by the Hamiltonian of specific models. In next subsection, we will write O_i and give J_i for a general multiband model.

At DC limit, the imaginary part of $L_{ij}^{xx}(\omega=0)$ is zero, thus S_0 is determined by the real parts. For convenience, define

$$L_{ij}^0 \equiv \mathbf{Re}L_{ij}^{xx}(0), \tag{10}$$

then we have

$$S_0 \equiv \mathbf{Re}S(\omega=0) = -\frac{1}{T}\frac{L_{12}^0}{L_{11}^0}. \tag{11}$$

At AC limit, $L_{ij}^{xx}(\omega)$ is dominated by the imaginary part, with a $O(1/\omega)$ leading order,

$$\mathbf{Im}L_{ij}^{xx}(\omega) = \frac{T}{\omega}L_{ij}^* + O(\frac{1}{\omega^2}). \tag{12}$$

Using Lehnman's representation, it has been shown that L_{ij}^* defined above is, up to a factor of i, the expectation values of commutators between current and polarization operators[9,12,13], i.e.,

$$L_{ij}^* = i\langle[J_j^x, O_j^x]\rangle. \tag{13}$$

Consequently, TEP at AC limit is

$$S^* \equiv \mathbf{Re}S(\omega\to\infty) = -\frac{1}{T}\frac{L_{12}^*}{L_{11}^*}. \tag{14}$$

L_{ij}^* can be related to $\mathbf{Re}L_{ij}(\omega)$. Applying Kramers-Kronig relation and keeping the leading order in $1/\omega$, we have

$$L_{ij}^* = \frac{1}{\pi T}\int_{-\infty}^{\infty} d\omega \mathbf{Re}L_{ij}^{xx}(\omega). \tag{15}$$

Thus L_{ij}^* is also connected to the sum rules of dynamical quantities. For example, L_{11}^* is proportional to the sum rule of conductivity[18,19].

$$L_{11}^* = \frac{2}{\pi}\int_0^{\infty} d\omega \mathbf{Re}\sigma(\omega). \tag{16}$$

Other sum rules are also derived in Ref.[12] and[13].

B. General formula of L_{ij}^*

Now we explicitly evaluate the commutator in Eq. (13) for a general tight-binding Hamiltonian with local interaction, which will determine the AC limit of TEP in this system. We start with the following Hamiltonian

$$\begin{aligned} H &= -\sum_{ij,\mu\nu} t_{ij}^{\mu\nu} c_{i\mu}^\dagger c_{j\nu} + \sum_{i\mu}\epsilon_\mu c_{i\mu}^\dagger c_{i\mu} \\ &\quad + \sum_i \sum_{\alpha\beta\mu\nu} U_{\alpha\beta\mu\nu} c_{i\mu}^\dagger c_{i\beta}^\dagger c_{i\nu} c_{i\mu}. \end{aligned} \tag{17}$$

i, j are site indices. α, β, μ and ν denote local orbitals. $t_{ij}^{\mu\nu}$ is the hopping integral, and $U_{\alpha\beta\mu\nu}$ is the matrix element for Coulomb interaction between local orbitals. ϵ_μ is energy level of local orbitals. The particle polarization operator is

$$O_1^x = \sum_i R_i^x \sum_\mu c_{i\mu}^\dagger c_{i\mu}, \tag{18}$$

and the heat polarization operator is

$$\begin{aligned} O_2^x &= \sum_i R_i^x \left[-\frac{1}{2} \sum_{j,\mu\nu} \left(t_{ij}^{\mu\nu} c_{i\mu}^\dagger c_{j\nu} + t_{ji}^{\nu\mu} c_{j\nu}^\dagger c_{i\mu} \right) \right. \\ &\quad \left. + \sum_{\alpha\beta\mu\nu} U_{\alpha\beta\mu\nu} c_{i\mu}^\dagger c_{i\beta}^\dagger c_{i\nu} c_{i\mu} + \sum_\alpha \left(\epsilon_\alpha - \mu \right) c_{i\alpha}^\dagger c_{i\alpha} \right]. \end{aligned} \tag{19}$$

The current operators turn out to be

$$\begin{aligned} J_1^x &= i[H, O_1^x] \\ &= -i \sum_{ij,\mu\nu} \left(R_j^x - R_i^x \right) t_{ij}^{\mu\nu} c_{i\mu}^\dagger c_{j\nu}, \end{aligned} \tag{20}$$

and

$$\begin{aligned} J_2^x &= i[H, O_2^x] \\ &= \sum_{ijl,\mu\nu\alpha} \frac{i}{2} t_{il}^{\mu\alpha} t_{lj}^{\alpha\nu} \left(R_j^x - R_i^x \right) c_{i\mu}^\dagger c_{j\nu} \\ &\quad -\frac{i}{2} \sum_{ij,\alpha\beta} t_{ij}^{\alpha\beta} \left(R_j^x - R_i^x \right) \left(\epsilon_\alpha + \epsilon_\beta - 2\mu \right) c_{i\alpha}^\dagger c_{j\beta} \\ &\quad -\frac{i}{2} \sum_{ij,\mu\nu} t_{ij}^{\mu\nu} \left(R_j^x - R_i^x \right) \\ &\quad \times \left(\sum_{\alpha'\mu'\nu'} \left(U_{\nu\alpha'\mu'\nu'} - U_{\alpha'\nu\mu'\nu'} \right) c_{i\mu}^\dagger c_{j\alpha'}^\dagger c_{j\nu'} c_{j\mu'} \right. \\ &\quad \left. + \sum_{\alpha'\beta'\nu'} \left(U_{\alpha'\beta'\mu\nu'} - U_{\alpha'\beta'\nu'\mu} \right) c_{i\alpha'}^\dagger c_{i\beta'}^\dagger c_{i\nu'} c_{j\nu} \right). \end{aligned} \tag{21}$$

In the literature[20], J_2^x is also written in a more compact form using the equation of motion in Heisenberg picture,

$$J_2^x = -\frac{1}{2} \sum_{ij,\mu\nu} \left(R_j^x - R_i^x \right) t_{ij}^{\mu\nu} \left(\dot{c}_{i\mu}^\dagger c_{j\nu} - c_{i\mu}^\dagger \dot{c}_{j\nu} \right),$$

in which the dot means the time derivative,

$$\dot{c}_{i\mu}^\dagger = i[H, c_{i\mu}^\dagger].$$

To compute L_{11}^* and L_{12}^*, we need to further evaluate the commutators between current operators and polarization operators. For L_{11}^*, this is simple and straightforward,

$$L_{11}^* = \sum_{ij,\mu\nu} t_{ij}^{\mu\nu} \left(R_j^x - R_i^x \right)^2 \langle c_{i\mu}^\dagger c_{j\nu} \rangle. \tag{22}$$

However, L_{12}^* leads to a complicate formula,

$$\begin{aligned} L_{12}^* &= -\sum_{ijl,\mu\nu\alpha} \frac{1}{2} t_{il}^{\mu\alpha} t_{lj}^{\alpha\nu} \left(R_j^x - R_i^x\right)^2 \langle c_{i\mu}^\dagger c_{j\nu}\rangle \\ &+\frac{1}{2}\sum_{ij,\mu\nu} t_{ij}^{\mu\nu} \left(R_j^x - R_i^x\right)^2 (\epsilon_\mu + \epsilon_\nu - 2\mu) \langle c_{i\mu}^\dagger c_{j\nu}\rangle \\ &+\frac{1}{2}\sum_{ij,\mu\nu} t_{ij}^{\mu\nu} \left(R_j^x - R_i^x\right)^2 \\ &\times \left(\sum_{\alpha'\mu'\nu'} \left(U_{\nu\alpha'\mu'\nu'} - U_{\alpha'\nu\mu'\nu'}\right) \langle c_{i\mu}^\dagger c_{j\alpha'}^\dagger c_{j\nu'} c_{j\mu'}\rangle \right. \\ &\left. + \sum_{\alpha'\beta'\nu'} \left(U_{\alpha'\beta'\mu\nu'} - U_{\alpha'\beta'\nu'\mu}\right) \langle c_{i\alpha'}^\dagger c_{i\beta'}^\dagger c_{i\nu'} c_{j\nu}\rangle \right). \end{aligned} \tag{23}$$

But this formula can be significantly simplified if we look at the equation of motion for the following Greens's function,

$$G_{ji}^{\nu\mu}(\tau) = -\langle T_\tau c_{j\nu}(\tau) c_{i\mu}^\dagger\rangle. \tag{24}$$

T_τ is the time-ordering operator in imaginary time. Its equation of motion reads,

$$\begin{aligned} \frac{\partial G_{ji}^{\nu\mu}(\tau)}{\partial\tau} &= \sum_{j'\nu'} t_{jj'}^{\nu\nu'} G_{j'i}^{\nu'\mu}(\tau) - (\epsilon_\nu - \mu) G_{ji}^{\nu\mu}(\tau) \\ &- \sum_{\alpha'\mu'\nu'} \left(U_{\alpha'\nu\mu'\nu'} - U_{\nu\alpha'\mu'\nu'}\right) \\ &\times \langle T_\tau c_{j\alpha'}^\dagger(\tau) c_{j\nu'}(\tau) c_{j\mu'}(\tau) c_{i\mu}^\dagger\rangle. \end{aligned}$$

Taking the $\tau \to 0^-$ limit leads to

$$\begin{aligned} &\sum_{\alpha'\mu'\nu'} \left(U_{\nu\alpha'\mu'\nu'} - U_{\alpha'\nu\mu'\nu'}\right) \langle c_{i\mu}^\dagger c_{j\alpha'}^\dagger c_{j\nu'} c_{j\mu'}\rangle \\ &= -\lim_{\tau\to 0^-} \frac{\partial G_{ji}^{\nu\mu}(\tau)}{\partial\tau} + \sum_{j'\nu'} t_{jj'}^{\nu\nu'} \langle c_{i\mu}^\dagger c_{j'\nu'}\rangle \\ &- (\epsilon_\nu - \mu) \langle c_{i\mu}^\dagger c_{j\nu}\rangle. \end{aligned} \tag{25}$$

Substituting the last term in Eq. (23) by the right hand side of Eq. (25), we get

$$\begin{aligned} L_{12}^* = -\frac{1}{2}\sum_{ijl,\mu\nu\alpha} t_{il}^{\mu\alpha} t_{lj}^{\alpha\nu} &\left[\left(R_j^x - R_i^x\right)^2 \right. \\ &\left. - (R_l^x - R_i^x)^2 - \left(R_j^x - R_l^x\right)^2 \right] \langle c_{i\mu}^\dagger c_{j\nu}\rangle \\ &- \sum_{ij,\mu\nu} t_{ij}^{\mu\nu} \left(R_j^x - R_i^x\right)^2 \lim_{\tau\to 0^-} \frac{\partial}{\partial\tau} G_{ji}^{\nu\mu}(\tau). \end{aligned} \tag{26}$$

Using the fact that

$$\langle c_{i\mu}^\dagger c_{j\nu}\rangle = \lim_{\tau\to 0^-} G_{ji}^{\nu\mu}(\tau),$$

and performing Fourier transformation in both real space and imaginary time, we get

$$L_{11}^* = \frac{1}{\beta}\sum_{\omega_n} e^{-i\omega_n 0^-} \sum_{k,\mu\nu} \left(\frac{\partial^2 \epsilon_k^{\mu\nu}}{\partial k_x^2}\right) G_k^{\nu\mu}(i\omega_n), \tag{27}$$

and,

$$L_{12}^{*} = \frac{1}{\beta}\sum_{\omega_n} e^{-i\omega_n 0^-}\sum_{k,\mu\nu}\left[\sum_{\alpha}\left(\frac{\partial\epsilon_k^{\mu\alpha}}{\partial k_x}\right)\left(\frac{\partial\epsilon_k^{\alpha\nu}}{\partial k_x}\right) + i\omega_n\left(\frac{\partial^2\epsilon_k^{\mu\nu}}{\partial k_x^2}\right)\right] G_k^{\nu\mu}(i\omega_n). \quad (28)$$

$\epsilon_k^{\mu\nu}$ is Fourier transformation of hopping amplitudes,

$$\epsilon_k^{\mu\nu} = -\sum_R e^{ikR} t^{\mu\nu}(R), \quad (29)$$

where we have utilized the translational invariance,

$$t_{ij}^{\mu\nu} = t^{\mu\nu}(R_j - R_i). \quad (30)$$

It is straightforward to convert the Matsubara summation to the integration in real frequencies.

$$L_{11}^{*} = \int_{-\infty}^{\infty} d\omega \sum_{k,\mu\nu}\left(\frac{\partial^2\epsilon_k^{\mu\nu}}{\partial k_x^2}\right) f(\omega) A_k^{\nu\mu}(\omega), \quad (31)$$

and

$$L_{12}^{*} = \int_{-\infty}^{\infty} d\omega \sum_{k,\mu\nu}\left[\sum_{\alpha}\left(\frac{\partial\epsilon_k^{\mu\alpha}}{\partial k_x}\right)\left(\frac{\partial\epsilon_k^{\alpha\nu}}{\partial k_x}\right) + \omega\left(\frac{\partial^2\epsilon_k^{\mu\nu}}{\partial k_x^2}\right)\right] f(\omega) A_k^{\nu\mu}(\omega). \quad (32)$$

$f(\omega) = 1/(1+\exp(\beta\omega))$ is the Fermi function. $A_k^{\nu\mu}(\omega) = -\frac{1}{\pi}G_k^{\nu\mu}(\omega)$ is the spectral function.

Eq. (27), Eq. (28), Eq. (31) and Eq. (32) are main results in this work. They are derived from a general formalism of dynamical thermoelectric transport outline in Sec. II A and a multiband Hamiltnian, Eq. (17). The equation of motion is exact and no approximation is assumed in the derivation. These equations indicate that L_{11}^{*} and L_{12}^{*}, and thus S^{*} are determined by the non-interacting band structure and the single-particle spectral fundtion.

III. S_0 AND S^{*} IN A ONE-BAND HUBBARD MODEL

In this section, we discuss S_0 and S^{*} of one-band Hubbard model in the scenario of dynamical mean field theory(DMFT), using the formalism we presented in previous sections.

The Hamiltonian of one-band Hubbard model is

$$H = -\sum_{ij,\sigma} t_{ij} c_{i\sigma}^{\dagger} c_{j\sigma} + U\sum_i n_{i\uparrow} n_{i\downarrow}. \quad (33)$$

In DMFT, it is mapped to a single-impurity Anderson model[21] supplemented by the self-consistent condition, which reads,

$$\frac{1}{i\omega_n + \mu - \Delta(i\omega_n) - \Sigma(i\omega_n)} = \sum_k G_k(i\omega_n). \quad (34)$$

On the left hand side is the local Green's function on the impurity. $\Delta(i\omega_n)$ is the hybridization function of the impurity model. On the right hand side, $G_k(i\omega_n)$ is the Green's function of lattice electrons,

$$G_k(i\omega_n) = \frac{1}{i\omega_n + \mu - \epsilon_k - \Sigma(i\omega_n)},$$

with ϵ_k the non-interacting dispersion relation of the lattice model, and $\Sigma(i\omega_n)$ the self energy for both local and lattice Green's function in the self-consistent condition. In DMFT, both coherent and incoherent excitations in a correlated metal are treated on the same footing[22].

In DMFT, the evaluation of transport coefficients,e.g., Eq. (6), can be significantly simplified. Because the k-dependence falls solely on the non-interacting dispersion ϵ_k, the vertex corrections vanishes[23]. Consequently, $\mathbf{Re}L_{ij}(\omega)$ can be written in terms of single-particle spectral function in real frequency.

$$\begin{aligned}\mathbf{Re}L_{ij}(\omega) &= \pi T\sum_{k,\sigma}\left(\frac{\partial\epsilon_k}{\partial k_x}\right)^2\int_{\infty}^{\infty}d\omega'(\omega'+\frac{\omega}{2})^{i+j-2}\\ &\times\left(\frac{f(\omega')-f(\omega'+\omega)}{\omega}\right)A_k(\omega')A_k(\omega'+\omega).\end{aligned} \tag{35}$$

Notice that here the dependence of $\mathbf{Re}L_{ij}(\omega)$ on the single-particle spectral function is generally approximate for a finite-dimensional system, which is achieved due to the vanishing of vertex corrections exact only in infinite dimensions. But the dependence of L^*_{ij} on single-particle spectral function is exact, as pointed out at the end of Sec. II A.

Another question is on the sum rule of the approximate $\mathbf{Re}L_{ij}(\omega)$, i.e., if we substitute Eq. (35) into the definition of L^*_{ij}, Eq. (15), wether or not it will give the same form of L^*_{ij} as we have derived in last section. The answer to this question is yes and we a brief proof for this one-band case in the Appendix but the extension to multiband case is straightforward. This means that ignoring vertex correction will modify the distribution of weight in $\mathbf{Re}L_{ij}(\omega)$, but will not change the integrated weight.

The DC limit of $\mathbf{Re}L_{ij}(\omega)$, L^0_{ij} can be obtained by takeing the limit $\omega\to 0$, which gives,

$$L^0_{ij}=\pi T\sum_{k,\sigma}\left(\frac{\partial\epsilon_k}{\partial k_x}\right)^2\int_{-\infty}^{\infty}d\omega\omega^{i+j-2}\left(-\frac{\partial f(\omega)}{\partial\omega}\right)A_k(\omega)^2. \tag{36}$$

Therefore in the framework of DMFT, S_0 is computed from Eq. (36). The AC limit, S^* can be computed from Eq. (27) and Eq. (28), or Eq. (31) and Eq. (31). In principle, Matsubara frequency and integration over real frequency give identical results. But in practice, especially in numerical computations on correlated systems, correlation functions in Matsubara frequencies are more easily accessible. For example, among various impurity solvers in DMFT, quantum Monte Carlo method(QMC), i.e., Hirsch-Fye method[24] and recently developed continuous time QMC[25,26] are implemented in imaginary time. To get correlation functions in real frequencies, numerical realization of analytical continuation has to be employed, such as maximum entropy method, which is a involved procedure and usually special care has to be taken of. In this case, a formulae in Matsubara frequencies will significantly simplify the calculation.

Due to the bad convergence of the series, Eq. (27) and Eq. (28) are not appropriate for direct implementation into numerical computations. Following standard recipe(separating and analytically evaluating the badly convergent part), we transform them in a form more friendly to numerics. For the one-band Hubbard model,

$$L^*_{11}=\sum_{k,\sigma}\left(\frac{\partial^2\epsilon_{k\sigma}}{\partial k_x^2}\right)\left(\frac{1}{\beta}\sum_{\omega_n}\mathbf{Re}G_k(i\omega_n)-\frac{1}{2}\right), \tag{37}$$

and

$$L^*_{12} = \sum_{k,\sigma}\left(\frac{\partial\epsilon_k}{\partial k_x}\right)^2\frac{1}{\beta}\sum_{\omega_n}\mathbf{Re}G_k(i\omega_n)\times\left[1+2\omega_n\mathbf{Im}G_k(i\omega_n)\right]. \tag{38}$$

A. Low temperature limit.

At low temperatures(low-T), the derivative of Fermi function, $(-\partial f(\omega)/\partial\omega)$ in the integrand of Eq. (36) becomes Dirac-δ function-like, thus only the low energy part of the spectral weight near Fermi surface contributes to the integral. The low energy part of the self energy of a Fermi liquid $\Sigma(\omega)$ can be approximated by a Taylor expansion in terms of ω and T.

$$\begin{aligned}\mathbf{Re}\Sigma(\omega) &\simeq \left(1-\frac{1}{Z}\right)\omega,\\ \mathbf{Im}\Sigma(\omega) &\simeq \frac{\gamma_0}{Z^2}(\omega^2+\pi^2T^2)+\frac{1}{Z^3}(a_1\omega^2+\omega T^2).\end{aligned}$$

Previous studies[8,27] showed that at low-T limit, $L^0_{11}\propto Z^2/T$ and $L^0_{12}\propto ZT$, thus $S_0=-L^0_{12}/(TL^0_{11})\propto T/Z$.

Since we are interested in the relation between S_0 ad S^*, it would be convenient to write L^*_{12} and L^*_{11} in terms of the conventional transport function, $(\partial\epsilon_k/\partial k_x)^2$. This can be achieved by performing integration by part on the summation over k in in Eq. (31) and Eq. 32, then we have

$$L^*_{ij} = L^*_{ij,I} + L^*_{ij,II},$$

with

$$\begin{aligned} L^*_{ij,I} &= \sum_{k,\sigma}\left(\frac{\partial\epsilon_k}{\partial k_x}\right)^2 \int d\omega \left(-\frac{\partial f(\omega)}{\partial\omega}\right) \\ &\quad \times\omega^{i+j-2}\left(-\frac{1}{\pi}\right)\mathbf{Im}\left[G_k(\omega)Z(\omega)\right], \end{aligned} \tag{39}$$

$$\begin{aligned} L^*_{ij,II} &= \sum_{k,\sigma}\left(\frac{\partial\epsilon_k}{\partial k_x}\right)^2 \int d\omega f(\omega)\left(-\frac{1}{\pi}\right) \\ &\quad \times\mathbf{Im}\left[G(\epsilon,\omega)\frac{\partial}{\partial\omega}\left(\omega^{i+j-2}(1-Z(\omega))\right)\right], \end{aligned} \tag{40}$$

where we have defined

$$Z(\omega) = \frac{1}{1-\partial\Sigma(\omega)/\partial\omega}.$$

We introduced the function $Z(\omega)$, which is dependent on the derivative of self energy with respect to energy ω. The integrand in $L^*_{ij,I}$(Eq.(39)) also has the derivative of Fermi function. Also notice that at low-T, $Z(\omega=0)=Z$, which is the renormalization factor of correlated Fermi liquid. Then $L^*_{ij,I}$ resembles L^0_{12} except for the power of $\mathbf{Im}G_k(\omega)$. Low temperature expansion show that $L^*_{11,I}\propto Z$, and $L^*_{12,I}\propto T^2$. Therefore, if $L^*_{11,II}$ and $L^*_{12,II}$ were absent, $S^* = -(TL^*_{12,I})/L^*_{11,I}\propto T/Z$, which is similar to the low-T behavior of S_0.

However, $L^*_{11,II}$ and $L^*_{12,II}$ do not vanish in general at low-T limit. First, at low-T limit, the integral over ω in Eq. (40)

$$\int_{-\infty}^{\infty} d\omega f(\omega) \quad \text{is replaced by} \quad \int_{-\infty}^{0} d\omega.$$

Then both the real and imaginary part of $G_k(\omega)$ and $Z(\omega)$ below Fermi surface have to contribute to the leading order of $L^*_{ij,II}$, unless $\Sigma(\omega)$ is independent, or at least weakly dependent on ω, leading $Z(\omega)\simeq 1$, and then the integrand in $L^*_{ij,II}$ would vanish. But this in general can not be true. For example, in a correlated Fermi liquid phase near the Mott transition of Hubbard model, $\Sigma(\omega)$ contains the information of coherent quasiparticles at Fermi surface as well as that of incoherent excitations in high-energy Hubbard bands, thus $\Sigma(\omega)$ will depend on ω in very different ways at these separated energy scales. At low energy scale, $Z(\omega\simeq 0)\simeq Z$, and Z is significantly less than 1 near Mott transition. Therefore, at low-T limit, $L^*_{ij,II}$ will exhibit a finite value at low-T limit. So the total value of L^*_{12} will be dominated by $L^*_{12,II}$ instead of the $\sim T^2$ contribution from $L^*_{12,I}$. The finiteness of L^*_{11} can be also justified by the general sum rule Eq. (31), which indicates that L^*_{11} is proportional to the kinetic energy. Consequently, S^* will diverge $1/T$-like at low-T limit for a correlated Fermi liquid.

There are some circumstances in which $Z(\omega)=1$ and $L^*_{ij,II}$ vanishes. One example is that in a static mean field theory, such as Hartree-Fock approximation, $\Sigma(\omega)$ is independent on ω, thus in static mean field theory, it is possible that S^* can show a similar behavior to that of S_0 at low temperature.

B. High temperature limit.

In the literature, the high temperature limit of thermopower[4], or known as Mott-Heikes formulor, has been widely used as a benchmark for thermoelectric capability[6] for correlated materials. Here we discuss the high temperature limit of S^* implied from the formulae we have derived.

The high temperature limit relevant for correlated systems was approached by first taking the limit $U\to\infty$, which excludes the double- occupancy in hole-doped systems or the vacancy in electron-doped systems, then taking the high

temperature limit $T \to 0$. This leads to two major simplification. First, by definition in thermodynamics,

$$\frac{\mu}{T} = -\left(\frac{\partial s}{\partial N}\right)_{E,V}.$$

Here s is the entropy and N is number of electrons. s can be calculated by counting all possible occupation states satisfying the $U \to \infty$ limit. It turns out that $\frac{\mu}{T}$ is a constant determined by the electron density. Thus μ is proportional to T at high temperature. The second simplification is that at high temperature, we can approximate the single particle spectral function by a rigid band picture, namely,

$$\tilde{A}_k(\omega) = A_k(\omega - \mu). \tag{41}$$

$\tilde{A}_k(\omega)$ is a function of ω but independent of temperature and chemical potential. Applying these simplification to Eq. (31) and Eq. (32), and keeping the leading order in T, we have

$$\begin{aligned} L_{11}^* &= \frac{1}{1+e^{-\beta\mu}} \int d\omega \sum_{k,\sigma} \left(\frac{\partial^2 \epsilon_k}{\partial k_x^2}\right) \tilde{A}_k(\omega), \\ L_{12}^* &= \frac{-\mu}{1+e^{-\beta\mu}} \int d\omega \sum_{k,\sigma} \left(\frac{\partial^2 \epsilon_k}{\partial k_x^2}\right) \tilde{A}_k(\omega). \end{aligned}$$

Therefore, at high temperature limit,

$$S^* = -\frac{L_{12}^*}{T L_{11}^*} = \frac{\mu}{T}. \tag{42}$$

This is the same result to the high temperature limit of S_0 in Ref.[4]. Thus the leading order of S^* is identical to the leading order of S_0 at high temperature.

IV. NUMERICAL RESULTS

In this section, we compute the dynamical thermoelectric power $S(\omega)$ by dynamical mean field theory(DMFT). We use exact diagonalization(ED) as the impurity solver. The advantage of the ED solver is the Green's functions can be computed simultaneously in real and Matsubara frequencies. Thus we have two approaches to compute the AC limit S^*. The first one is to substitute the Green's function in Matsubara frequencies into Eq. (27) and Eq. (28). The second method starts from computing $\mathbf{Re}L_{11}(\omega)$ and $\mathbf{Re}L_{12}(\omega)$ from spectral functions $A_k(\omega)$ using Eq. (35) for a wide range of ω, Kramers-Kronig relation is implemented to compute $\mathbf{Im}L_{11}(\omega)$ and $\mathbf{Im}L_{12}(\omega)$, and finally with the value of L_{11}^* and L_{12}^* obtained by fitting Eq. (12) at the $\omega \to \infty$ limit. The second method is more laborious but here we use it as a check for our formulae in Matsubara frequencies.

We study one-band Hubbard model on square and triangular lattices and consider only the hopping between nearest neighboring sites.

A. Square lattice

In this section, we compute the thermoelectric transport coefficients and thermoelectric power for a hole-doped Hubbard model on square lattice. We use the bandwidth D as the unit for frequency ω, temperature T and interaction strength U. For square lattice, $D = 8|t|$, t is the hopping constant.

In Fig. 1 we show the frequency-dependent quantities for $U = 1.75D$ and $n = 0.85$. Fig. 1-(a) and -(b) show the thermoelectric transport coefficients $L_{11}(\omega)$ and $L_{12}(\omega)$ by their real(red line) and imaginary part(black line). The real parts are computed from Eq. (35). The imaginary parts are computed from Kramers-Kronig relation. Three contributions are recognizable in $\mathbf{Re}L_{11}$: i) The low frequency peak due to transition within the resonance peak of quasiparticles. ii) The transition between quasiparticles and the lower Hubbard band, which accounts for the hump at $\omega \sim 0.5D$. iii) The weight around $\omega \sim U$, which is due to the incoherent excitations between Hubbard bands. Same features also exist in $\mathbf{Re}L_{12}(\omega)$, but the feature near $\omega \sim 0$ i.e., transition between quasiparticles, and the transition between quasiparticles and lower Hubbard band, are much less obvious. This is because the DC limit L_{12}^0 is dominated by the particle-hole asymmetry of the band velocity $\partial\epsilon_k/\partial k_x$ and the spectral function $A_k(\omega)$, due to the $\omega^{i+j-2} = \omega$ term in the integrand of Eq. (36) for L_{12}^0. Thus at small ω, $\mathbf{Re}L_{12}(\omega)$ is significantly impaired, compared

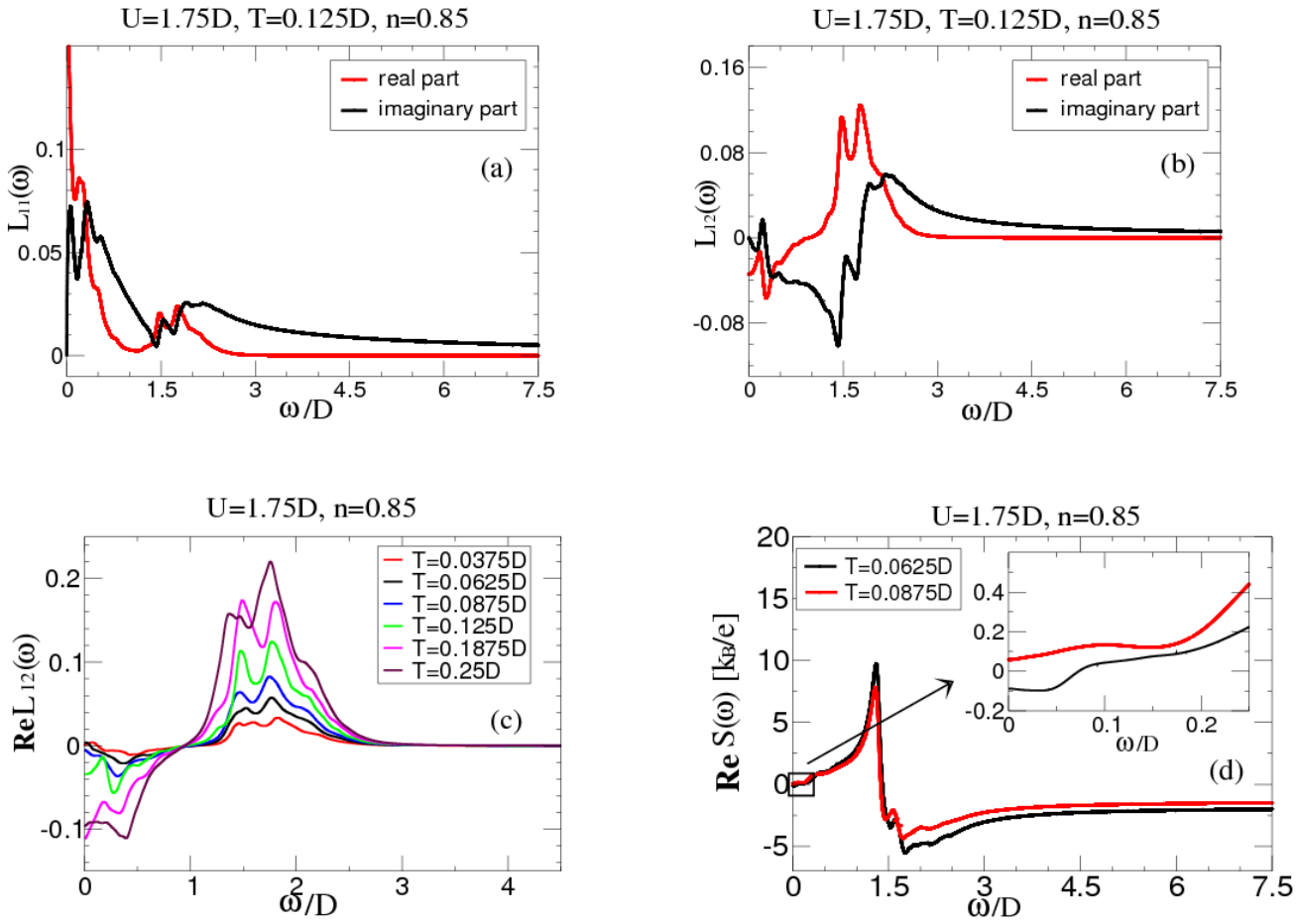

FIG. 1: Frequency-dependent transport coefficients and thermoelectric power of a hole-doped one-band Hubbard model on square lattice. $U = 1.75D$ and $n = 0.85$. (a) $\mathbf{Re}L_{11}(\omega)$ and $\mathbf{Im}L_{11}(\omega)$ at $T = 0.125D$. (b) $\mathbf{Re}L_{12}(\omega)$ and $\mathbf{Im}L_{12}(\omega)$ at $T = 0.125D$. (c) The evolution of $\mathbf{Re}L_{12}(\omega)$ with temperature. (d) $\mathbf{Re}S(\omega)$ at $T = 0.0625D$ and $T = 0.0875D$. The inset blows up the region near $\omega = 0$.

to $\mathbf{Re}L_{11}(\omega)$. Therefore the transition by incoherent excitations around $\omega \sim U$ takes a major part in the total weight in $\mathbf{Re}L_{12}(\omega)$, and the sum rule of $\mathbf{Re}L_{12}(\omega)$, i.e., L^*_{12}, is also dominated by the incoherent excitations. $\mathbf{Im}L_{11}(\omega)$ and $\mathbf{Im}L_{12}(\omega)$ are odd functions of ω and vanish at $\omega = 0$. It is evident that the real parts approach to zero much faster than the imaginary parts at AC limit($\omega \to \infty$),. Fig. 1-(c) shows the evolution of $\mathbf{Re}L_{12}(\omega)$ as temperatures. The dominance of the incoherent excitations is robust as the variation of temperature. Fig. 1-(d) shows the real part of thermoelectric power, $\mathbf{Re}S(\omega)$ for $T = 0.0625D$ and $T = 0.0875D$. The inset blows up the region near $\omega = 0$, indicating that S_0 displays + or − signs at different temperatures.

In Fig. 2-(a) and (b) we show S_0 and S^* at various temperatures. On the one side, in Fig. 2-(a), S_0 presents multiple changes of sign with temperature increased. The sign change at lower temperature($T \sim 0.1D$) demonstrates the crossover from the low-temperature hole-like coherent quasiparticles to incoherent excitations at intermediate temperature. Around $T = 0.2D$, where S_0 reaches its maximum positive value, where the coherent quasiparticles have almost diminished. The second sign change around $T = 0.6D$ indicates a subtle competition between the spectral weight of lower and higher Hubbard band. As temperature increases, the asymmetry between the two Hubbard bands near Fermi surface becomes less significant because more spectral weight from the higher Hubbard band takes part into the transport and the sign of S_0 is determined by the difference between the weight of lower and higher Hubbard. This crossover is thus considered to be responsible for the second sign change[9] and also has been observed experimentally[28]. Therefore, above $T = 0.6D$, the transport is completely dominated by incoherent excitations from both Hubbard bands. On the other side, in Fig. 2-(b), the situation for S^* is quite different. S^* does not change sign and keeps negative in the shown temperature range. Towards low temperature, S^* blows up, consistent with our

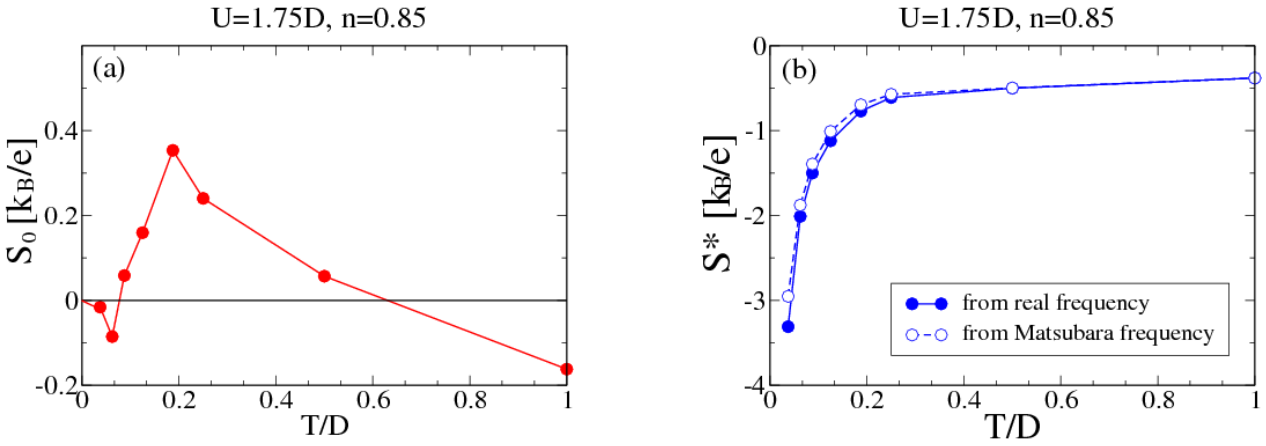

FIG. 2: (a): Temperature dependence of S_0. (b): Temperature dependence of S^* obtained from real frequencies (filled circles) and from Matsubara frequencies (open circles). Square lattice.

argument based on a Fermi liquid self energy in Sec. III A. Towards high temperature, i.e., when the temperature is well above the coherence regime, S_0 and S^* have the same sign and similar magnitude. We notice that S_0 in Fig. 2-(a) does not converge to the value predicted by the Mott-Heikes formula in the correlated regime($S_{MH} \simeq 1.04 k_B/e$, from Eq. (11) in Ref.[4]). This is because in our case, with $U = 1.5D$, the requirement for $|t| \ll T \ll U$ can not be satisfied for a wide range of temperature. Thus at high temperature, e.g., when $T > 0.6D$, the states with double occupancy can not be excluded and they are responsible for the second sign change in S_0 as discussed above.

In Fig. 2-(b), we show S^* obtained by the two methods mentioned at the beginning of Sec. IV. The solid circles represents S^* by fitting $\mathbf{Im}L_{11}(\omega)$ and $\mathbf{Im}L_{12}(\omega)$ in real frequency at $\omega \to \infty$ limit. The open circles represent S^* computed using Eq. (27) and Eq. (28). The values of S^* at open and closed circles are very close, indicating the consistency between the real and Matsubara frequency approach to calculate S^*.

The dependence on electron density of S_0 and S^* is more non-trivial, which is difficult to tell from analytical formulas. Fig. 3 shows S_0 and S^* at various densities for $U = 1.75D$. S_0 changes sign from positive at half filling to negative as electron density decreases, while S^* remains negative. The behavior of S_0 here is also due to the breakdown of coherence as the evolution of spectral weight. In a doped Mott insulator, the quasiparticle peak gradually diminishes as the system is doped away from half-filling[29]. Thus near half-filling, the transport is dominated by the coherent excitations near Fermi surface. But when the doping is heavy enough to kill quasiparticles, transport is carried by incoherent excitations in the Hubbard bands. Therefore S_0 turns to a same sign with S^*, since S^* is dominated by the Hubbard bands(see Fig. 1-(c) and discussion there). In Fig. 3 we also put the results of S^* by real and Matsubara frequency approach.

B. Triangular lattice

Recent interest on thermoelectric performance of correlated systems was attributed to the discovery of TEP enhancement in highly electron doped cobaltates[30]. The Co atoms in the CoO_2 layers form a triangular lattice. The physics behind the large TEP in Na_xCoO_2 is highly non-trivial. For example, the Na potential is crucial to induce the correlation in $Na_{0.7}CoO_2$[31], and the spin and orbital degrees of freedom are argued to be a key factor for the enhancement[6,32]. These complexities are beyond a single band Hubbard on a triangular lattice. Here we only focus on some qualitative features of S_0 and S^* in a electron-doped single band Hubbard model on triangular lattice.

In triangular lattice, $U = 12|t|$ and we use a positive t. S^* in this section is solely computed by using Eq. (27) and Eq. (27).

Fig. 4-(a) and -(b) shows the density dependence of S_0 and S^* for two different interaction strength. Here we present the full range for electron doping. Here S^* is from the summation over Matsubara frequency. For $U = 1.25D$(Fig. 4-(a)), S_0 is negative near half-filling and changes to positive after a small amount of doping. As the density approaches to band insulator($n = 2$), the merging of S_0 and S^* is very evident. For smaller interaction strength, i.e., $U = 0.5D$, S_0 and S^* also display similar trend through the range of electron density. This behavior is similar to the case on square lattice, Fig. 3. The discrepancy between S_0 and S^* is most evident for $U = 1.25D$ and near half-filling($n = 1.0$), since

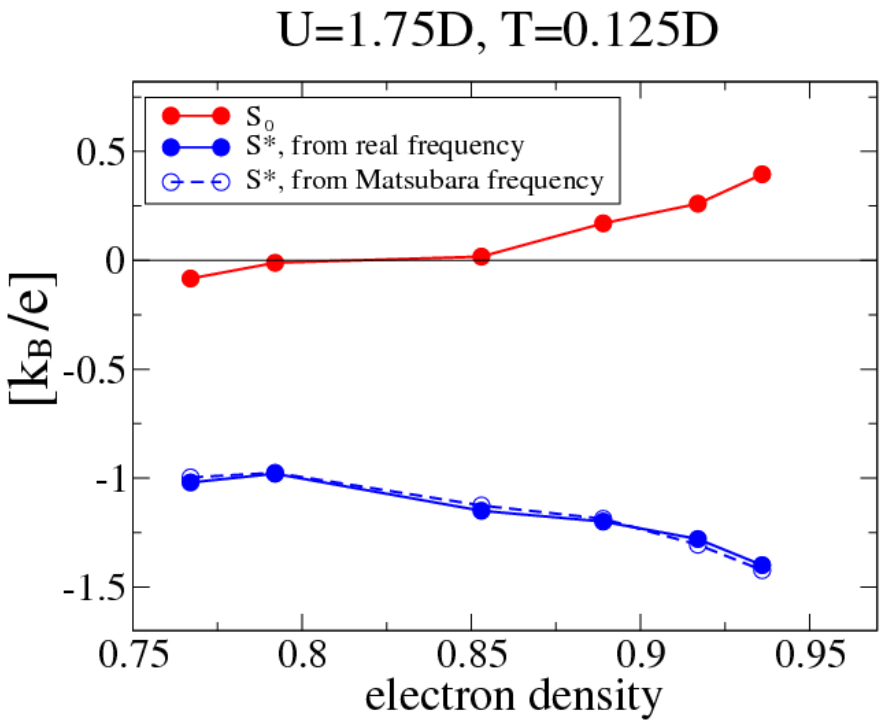

FIG. 3: Doping dependence of S_0 and S^* for $U = 1.75D$. S^* was obtained from real frequencies (filled circles) and Matsubara frequencies (open circles). The temperature here is $T = 0.125D$. Square lattice.

around this regime the coherent quasiparticles take a significant role in transport. For electron density larger than 1.5, which is the range of interest for cobaltate, the trend of S^* shows that it is a reasonable approximation to S_0.

V. SUMMARY

Using the formulae derived in Sec. II, we investigate to what extent the AC limit of thermoelectric power, S^*, can be a reasonable approximation to the DC limit, S_0. Analytical and numerical results on a single-band Hubbard model show that below and around coherent temperature, i.e., when the spectral weight around quasiparticle peak dominates in the thermoelectric transport, the behaviors of S_0 and S^* are significantly different. Specifically, S_0 displays multiple sign changes around the coherent temperature, but S^* does not. But when the temperature is well beyond the coherent regime, thus the transport properties are dominated by the incoherent excitations, S^* shows same sign and similar magnitude to S_0 and can give reasonable prediction on the behavior of S^*.

Our work suggest that a realistic implementation of Eq. (27) and Eq. (28) in LDA+DMFT codes can serve as a useful guide for the search of high performance thermoelectric materials among the strongly correlated electron systems, which have a very broad temperature regime characterized by incoherent transport.

At the time of writing, we are aware of a recent work by M. Uchida et al.[33], in which the incoherent thermoelectric transport over a wide temperature range is studied in a typical density-driven Mott transition system $La_{1-x}Sr_xVO_3$ and the validity of Mott-Heikes formula for real strongly correlated materials is verified.

VI. ACKNOWLEDGEMENT

This work was supported by the NSF under NSF grant DMR-0906943. CW was supported by the Swiss Foundation for Science (SNF). Useful discussions with K. Haule, V. Oudovenko and J. Tomczak are gratefully acknowledged.

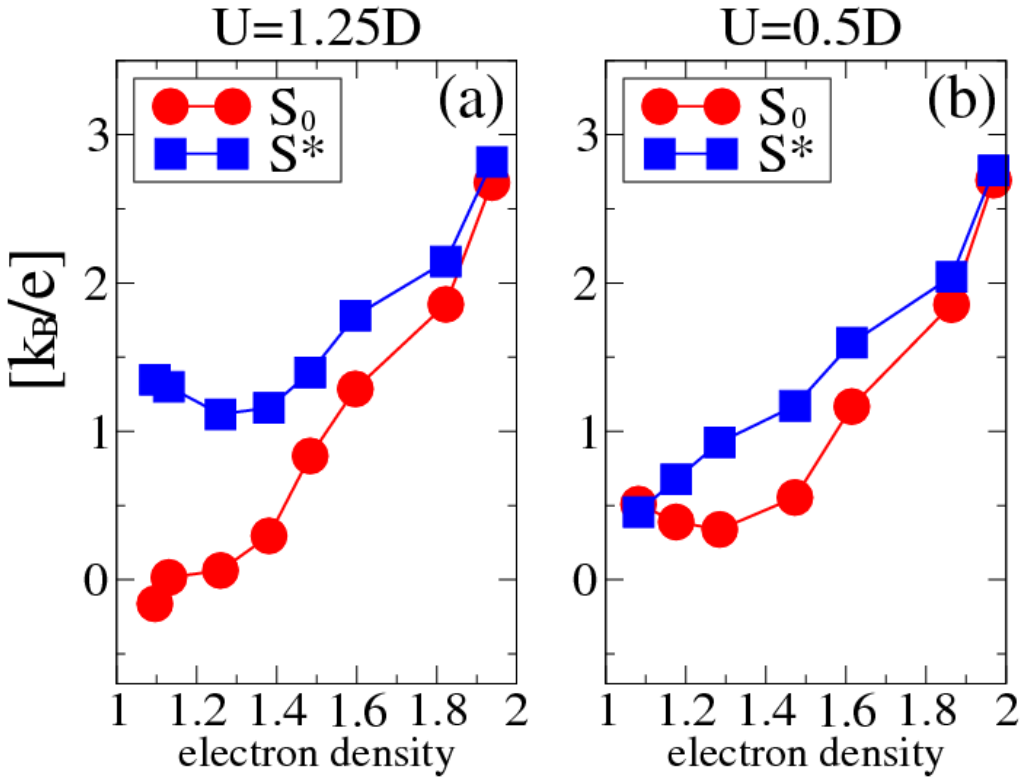

FIG. 4: (a) and (b): Density dependence of S_0 and S^* for $U = 1.25D$ and $U = 0.5D$. S^* was obtained from the Matsubara frequencies. Triangular lattice.

Appendix A: Sum rules for $\mathbf{Re}L_{12}(\omega)$ and $\mathbf{Re}L_{11}(\omega)$ in DMFT

In this appendix, we compute L^*_{11} and L^*_{12} in the framework of dynamical mean field theory and show they also obey the general formulae, Eq. (31 and Eq. (32).

In terms of retarded current-current correlations,

$$\mathbf{Re}L^{xx}_{12}(\omega) = -\frac{1}{\omega}\mathbf{Im}\left[\int_{-\infty}^{\infty} dt e^{i(\omega+i0^+)}\left[-i\theta(t)\langle[J_j(t), J_i]\rangle\right]\right], \tag{A1}$$

which can be computed in Matsubara frequencies by standard diagrammatic techniques[16]. In the infinite dimension limit, a significant simplification is achieved because all nonlocal irreducible vertex collapse and only the first bubble diagram survives[19,23]. This simplification leads to

$$\begin{aligned}\mathbf{Re}L^{xx}_{ij}(\omega) &= \pi T\sum_{k,\sigma}\left(\frac{\partial\epsilon_k}{\partial k_x}\right)^2\int_{\infty}^{\infty} d\omega'\left(\omega'+\frac{\omega}{2}\right)^{i+j-2} \\ &\times\left(\frac{f(\omega')-f(\omega'+\omega)}{\omega}\right)A_k(\omega')A_k(\omega'+\omega).\end{aligned} \tag{A2}$$

Now we calculate L^*_{ij}. Using Eq. (15),

$$L^*_{12} = \sum_{k,\sigma} \left(\frac{\partial \epsilon_k}{\partial k_x}\right)^2 \int d\omega d\omega' \left(\omega' + \frac{\omega}{2}\right) \times \left(\frac{f(\omega') - f(\omega+\omega')}{\omega}\right) A_k(\omega') A_k(\omega'+\omega). \quad \text{(A3)}$$

Changing variables by

$$\begin{aligned} \omega_1 &= \omega + \omega', \\ \omega_2 &= \omega, \end{aligned}$$

leads to

$$L^*_{12} = \sum_{k,\sigma} \left(\frac{\partial \epsilon_k}{\partial k_x}\right)^2 \int d\omega_1 d\omega_2 f(\omega_2) A_k(\omega_1) A_k(\omega_2) + 2\sum_{k,\sigma} \left(\frac{\partial \epsilon_k}{\partial k_x}\right)^2 \int d\omega_1 d\omega_2 \frac{\omega_2}{\omega_1 - \omega_2} f(\omega_2) A_k(\omega_1) A_k(\omega_2). \quad \text{(A4)}$$

The sum rule $\int d\omega_1 A_k(\omega_1) = 1$ simplifies the first term to

$$\sum_{k,\sigma} \left(\frac{\partial \epsilon_k}{\partial k_x}\right)^2 \int d\omega_2 f(\omega_2) A_k(\omega_2).$$

In the second term, Kramer-Kronig relation can be used to eliminate the integral over ω_1, i.e.,

$$\int d\omega_1 \frac{A_k(\omega_1)}{\omega_1 - \omega_2} = -\mathbf{Re} G_k(\omega_2).$$

Then we use the fact that

$$2\mathbf{Re} G_k(\omega) \mathbf{Im} G_k(\omega) = \mathbf{Im} G_k^2(\omega)$$

and

$$\frac{\partial}{\partial k_x} G_k(\omega) = G_k^2(\omega) \frac{\partial \epsilon_k}{\partial k_x},$$

to simplify the second term on the right hand side of Eq. (A4) to

$$\sum_{k,\sigma} \left(\frac{\partial \epsilon_k}{\partial k_x}\right) \int d\omega_2 \omega_2 f(\omega_2) \left(\frac{1}{\pi}\right) \frac{\partial}{\partial k_x} \mathbf{Im} G_k(\omega_2).$$

Applying integration by part over k, it turns out to be

$$\sum_{k,\sigma} \left(\frac{\partial^2 \epsilon_k}{\partial k_x^2}\right) \int d\omega_2 \omega_2 f(\omega_2) A_k(\omega_2).$$

Combined with the first term, we have

$$L^*_{12} = \sum_{k,\sigma} \int d\omega \left(\left(\frac{\partial \epsilon_k}{\partial k_x}\right)^2 + \omega \left(\frac{\partial^2 \epsilon_k}{\partial k_x^2}\right)\right) f(\omega) A_k(\omega). \quad \text{(A5)}$$

The calculation for L^*_{12} is similar and straightforward, which results in

$$L^*_{11} = \sum_{k,\sigma} \int d\omega \left(\frac{\partial^2 \epsilon_k}{\partial k_x^2}\right) f(\omega) A_k(\omega). \quad \text{(A6)}$$

---

[1] G. Mahan (Academic Press, 1997), vol. 51 of *Solid State Physics*, pp. 81 – 157.

[2] G. Mahan, B. Sales, and J. Sharp, Physics Today **50**, 42 (1997).
[3] G. J. Snyder and E. S. Toberer, Nature Mater. **7**, 105 (2008).
[4] P. M. Chaikin and G. Beni, Phys. Rev. B **13**, 647 (1976).
[5] G. Beni, Phys. Rev. B **10**, 2186 (1974).
[6] W. Koshibae, K. Tsutsui, and S. Maekawa, Phys. Rev. B **62**, 6869 (2000).
[7] H. Kontani, Phys. Rev. B **67**, 014408 (2003).
[8] G. Pálsson and G. Kotliar, Phys. Rev. Lett. **80**, 4775 (1998).
[9] V. S. Oudovenko and G. Kotliar, Phys. Rev. B **65**, 075102 (2002).
[10] S. Chakraborty, D. Galanakis, and P. Phillips, Phys. Rev. B **82**, 214503 (2010).
[11] M. R. Peterson and B. S. Shastry, Phys. Rev. B **82**, 195105 (2010).
[12] B. S. Shastry, Reports on Progress in Physics **72**, 016501 (2009).
[13] B. S. Shastry, Phys. Rev. B **73**, 085117 (2006).
[14] G. Kotliar, S. Y. Savrasov, K. Haule, V. S. Oudovenko, O. Parcollet, and C. A. Marianetti, Rev. Mod. Phys. **78**, 865 (2006).
[15] K. Held, R. Arita, V. I. Anisimov, and K. Kuroki, in *Properties and Applications of Thermoelectric Materials*, edited by V. Zlatic and A. C. Hewson (Springer Netherlands, 2009), NATO Science for Peace and Security Series B: Physics and Biophysics, pp. 141–157, ISBN 978-90-481-2892-1.
[16] G. D. Mahan, *Many-Particle Physics* (Plenum Press, New York, 1990).
[17] J. M. Luttinger, Phys. Rev. **135**, A1505 (1964).
[18] D. Pines and P. Noziéres, *The Theory of Quantum Liquids* (W. A. Benjamin, Inc., New York, 1966).
[19] M. J. Rozenberg, G. Kotliar, H. Kajueter, G. A. Thomas, D. H. Rapkine, J. M. Honig, and P. Metcalf, Phys. Rev. Lett. **75**, 105 (1995).
[20] I. Paul and G. Kotliar, Phys. Rev. B **67**, 115131 (2003).
[21] A. Georges and G. Kotliar, Phys. Rev. B **45**, 6479 (1992).
[22] A. Georges, G. Kotliar, W. Krauth, and M. J. Rozenberg, Rev. Mod. Phys. **68**, 13 (1996).
[23] T. Pruschke, D. L. Cox, and M. Jarrell, Phys. Rev. B **47**, 3553 (1993).
[24] J. E. Hirsch and R. M. Fye, Phys. Rev. Lett. **56**, 2521 (1986).
[25] P. Werner, A. Comanac, L. de' Medici, M. Troyer, and A. J. Millis, Phys. Rev. Lett. **97**, 076405 (2006).
[26] K. Haule, Phys. Rev. B **75**, 155113 (2007).
[27] K. Haule and G. Kotliar, in *Properties and Applications of Thermoelectric Materials*, edited by V. Zlatic and A. C. Hewson (Springer Netherlands, 2009), NATO Science for Peace and Security Series B: Physics and Biophysics, pp. 119–131, ISBN 978-90-481-2892-1.
[28] X. Yao, J. M. Honig, T. Hogan, C. Kannewurf, and J. Spałek, Phys. Rev. B **54**, 17469 (1996).
[29] H. Kajueter, G. Kotliar, and G. Moeller, Phys. Rev. B **53**, 16214 (1996).
[30] M. Lee, L. Viciu, L. Li, Y. Wang, M. L. Foo, S. Watauchi, R. A. Pascal Jr, R. J. Cava, and N. P. Ong, Nature Materials **5**, 537 (2006).
[31] C. A. Marianetti and G. Kotliar, Phys. Rev. Lett. **98**, 176405 (2007).
[32] Y. Wang, N. S. Rogado, R. J. Cava, and N. P. Ong, Nature **423**, 425 (2003).
[33] M. Uchida, K. Oishi, M. Matsuo, W. Koshibae, Y. Onose, M. Mori, J. Fujioka, S. Miyasaka, S. Maekawa, and Y. Tokura, cond-mat/1103.1185.